

# Sampling from Rough Energy Landscapes

Petr Plecháč, Gideon Simpson

---

## Abstract

Rough energy landscapes appear in a variety of applications including disordered media and soft matter. In this work, we examine challenges to sampling from Boltzmann distributions associated with rough energy landscapes. Here, the roughness will correspond to highly oscillatory, but bounded, perturbations of a smooth landscape. Through a combination of numerical experiments and asymptotic analysis we demonstrate that the performance of Metropolis Adjusted Langevin Algorithm can be severely attenuated as the roughness increases. In contrast, we prove, rigorously, that Random Walk Metropolis is insensitive to such roughness. We also formulate two alternative sampling strategies that incorporate large scale features of the energy landscape, while resisting the impact of roughness; these also outperform Random Walk Metropolis. Numerical experiments on these landscapes are presented that confirm our predictions. Open analysis questions and numerical challenges are also highlighted.

*Keywords:* Markov Chain Monte Carlo, random walk Metropolis, Metropolis adjusted Langevin, rough energy landscapes, mean squared displacement

*2000 MSC:* 65C05, 65C40, 60J22

---

## 1. Introduction

In this work, we consider the task of sampling from the Boltzmann distribution,

$$\mu(dx) = Z^{-1} e^{-\beta V(x)} dx, \quad Z = \int e^{-\beta V(x)} dx, \quad V : \mathbb{R}^n \rightarrow \mathbb{R}, \quad (1.1)$$

when  $V$  is, in some sense “rough,” or “rugged.” We are particularly interested in landscapes of the form

$$V_\epsilon(x) = V_0(x) + V_1(x, x/\epsilon). \quad (1.2)$$

Here,  $V_0$  is a smooth, long range, trapping potential ( $V_0(x) \rightarrow \infty$  as  $|x| \rightarrow \infty$ ) that is bounded from below, and  $V_1$  is bounded and includes local rough features.

---

*Email addresses:* [plechac@udel.edu](mailto:plechac@udel.edu) (Petr Plecháč), [grs53@drexel.edu](mailto:grs53@drexel.edu) (Gideon Simpson)

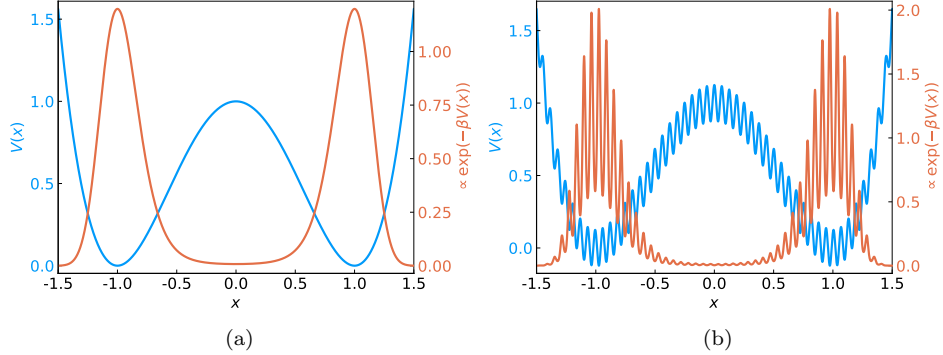


Figure 1: In (a), we see a smooth multimodal energy landscape. In contrast, the landscape in (b), is rough, with many internal energy barriers. The underlying potentials are  $V_0(x) = (x^2 - 1)^2$  and  $V_\epsilon(x) = V_0(x) + \frac{1}{8} \cos(x/\epsilon)$  with  $\epsilon = 0.01$  and  $\beta = 5$ . Color online.

Furthermore,  $V_1(x, y)$  will also be taken to be smooth. An example of such a rough landscape, and its impact on the associated distribution, is shown in Figure 1. Model potentials like (1.2) serve as prototypes for rough landscapes found in disordered media and soft matter, [1–5]. The goal of the present work is to assess how such roughness impacts the performance of well known Markov Chain Monte Carlo (MCMC) sampling strategies like Random Walk Metropolis (RWM) and Metropolis Adjusted Langevin (MALA).

Recall that RWM and MALA generate samples for  $e^{-\beta V(x)}$  with proposals

$$X_{k+1}^p = X_k + \sqrt{\beta^{-1}} \sigma \xi_{k+1}, \quad \xi_{k+1} \sim N(0, I), \quad (1.3)$$

$$X_{k+1}^p = X_k - \frac{\sigma^2}{2} \nabla V(X_k) + \sqrt{\beta^{-1}} \sigma \xi_{k+1}, \quad \xi_{k+1} \sim N(0, I). \quad (1.4)$$

These proposals are then accepted or rejected according to the appropriate rule to ensure detailed balance with respect to  $\mu(dx) \propto e^{-\beta V(x)} dx$ .

As an example, sample MALA paths with  $\sigma = 1$  for the landscapes in Figure 1 are shown in Figure 2. A path for the smooth landscape exhibits better mixing than the one for the rough landscape. On the rough landscape, the trajectory stagnates.<sup>1</sup> This begs the question of whether or not  $\sigma = 1$  was merely a poorly chosen value – perhaps with a different value, the rough landscape would also be efficiently sampled. Large values of  $\sigma$  result in proposals of greater magnitude, but few will be accepted, and the trajectory will move slowly. Conversely, small values of  $\sigma$  produce more readily accepted proposals, but their size limits exploration of the state space. Consequently, an optimal choice of  $\sigma$  is anticipated for each distribution.

Assuming we tune our sampler to the optimal  $\sigma$  for each  $V_\epsilon$ , we seek to assess how  $\epsilon$  impacts sampling performance. Ultimately, our work suggests that

<sup>1</sup> “Stagnation” corresponds to persistent rejection of proposals.

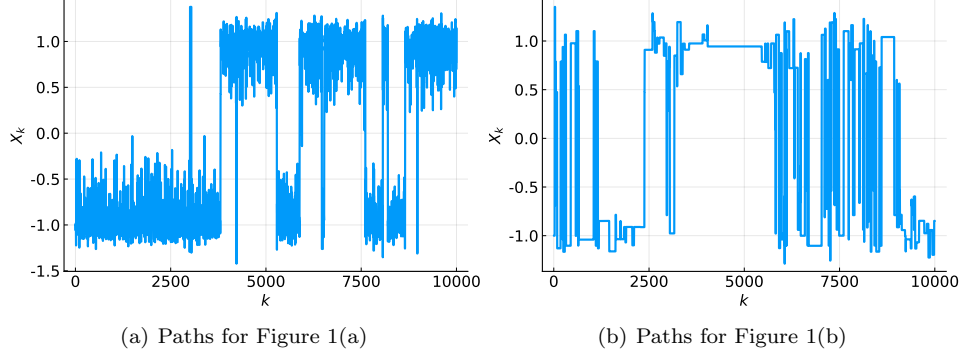


Figure 2: Sample paths corresponding to the energy landscapes in Figure 1. These were generated using MALA with  $\sigma = 1$ . Color online.

even for optimally tuned proposals, MALA will cease to be effective as  $\epsilon \rightarrow 0$ . In contrast, RWM remains robust. To obtain better performance than RWM, while still overcoming the robustness, we also formulate two related sampling strategies that incorporate information about the large scale (*i.e.* long wavelength) features of the energy landscape through  $V_0$  in (1.2). Indeed, our main analytic result, Theorem 1, shows that for potentials that can be decomposed as in (1.2) with  $V_0$  smooth and trapping and  $V_1$  rough but bounded, if the proposal of the sampling strategy is  $\epsilon$ -independent, then the performance of the method will also be  $\epsilon$ -independent.

### 1.1. Review of sampling strategies

The question of optimizing  $\sigma$  was initially examined in [6, 7] and has been subsequently studied in other works, including [8–16]. Many of these works consider energy landscape of the type

$$V(x) = \sum_{i=1}^n v(x_i), \quad x = (x_1, \dots, x_d) \in \mathbb{R}^d. \quad (1.5)$$

This choice of the potentials induces Boltzmann distributions that are products (for brevity, take  $\beta = 1$ ):

$$\mu(dx) \propto \prod_{i=1}^n e^{-v(x_i)} dx_i. \quad (1.6)$$

Thus, coordinates only interact through the accept/reject step of the method. Some results for potentials other than (1.5) (alternatively, (1.6)) have also been obtained. In [8], the authors treat distributions which have a density  $e^{-\Phi(x)}$  with respect to a separable measure (1.6).

In earlier works, [6–8], it was often assumed that whichever sampler is studied, the process is in stationarity. This has been relaxed in the more recent

results, [9–12, 15, 16]. In the case of (1.5), in stationarity, the performance can be measured by considering the means square displacement (MSD)

$$\text{MSD} = \mathbb{E}_\mu[|X_{n+1} - X_n|^2]. \quad (1.7)$$

Following the strategy of [8], we use the MSD as a proxy for the integrated autocorrelation, and  $\sigma$  is selected to maximize it in the limit of  $n \rightarrow \infty$ . Indeed, this leads to the results that, as  $n \rightarrow \infty$ ,

$$\text{MSD}/n = \ell^2 n^{-I} a(\ell; v) + o(n^{-I}) \quad (1.8)$$

where  $I > 0$  and  $a$  both depend on the method, but *not* the dimension  $n$ . The choice of  $\sigma$  is then related to  $\ell$  by

$$\sigma^2 = \ell^2 n^{-I} \quad (1.9)$$

The function  $a$  is actually the mean acceptance rate of the particular method in the  $n \rightarrow \infty$  limit.

Consequently, we can maximize this measure of performance as  $n \rightarrow \infty$  by solving

$$\ell_* = \operatorname{argmax}_\ell \ell^2 a(\ell; v). \quad (1.10)$$

The optimal  $\sigma_*$  is inferred from (1.9), and there is an associated optimal acceptance rate,  $a(\ell_*)$ . This optimization provides a strategy for tuning the value of  $\sigma$  to achieve the optimal acceptance rate approximately 23% for RWM. Analogously, one tunes MALA to have a 57% acceptance rate, [6, 7], and Hamiltonian Monte Carlo (HMC) to have a 65% acceptance rate, [14].

For RWM  $I = 1$  while it is  $I = 1/3$  for MALA. The function  $a$  has the explicit form

$$a(\ell; v) = 2\Phi\left(-\frac{\ell^{1/I}}{2}\sqrt{\mathcal{K}[v]}\right), \quad (1.11)$$

with  $\mathcal{K}$  a functional involving derivatives of  $v$ ;  $\Phi$  is merely the  $N(0, 1)$  cumulative distribution function. A similar result holds for HMC, [14].

There are caveats to applying these results in practical computations, [17]. In particular, the results are obtained as  $n \rightarrow \infty$  for distributions of form (1.6), and often assume the process to be in stationarity. Many distributions of interest will not be of this form, so target acceptance rates, like 23% for RWM, may be inappropriate.

We highlight, also, the recent work in [9], which studies “ridged” densities associated with potentials of the form

$$V_\epsilon(x) = V_0(x_1) + V_1(x_1, x_2/\epsilon), \quad x = (x_1, x_2) \in \mathbb{R}^{n=n_1+n_2}. \quad (1.12)$$

Here, roughness is only present in a subset of the degrees of freedom ( $x_2$ ). Examining RWM for such a problem, the authors are able to derive a limiting diffusion from which they can find an optimal step size. The limiting diffusion has a state dependent diffusion coefficient. Both the drift and diffusion coefficients are nontrivial, requiring averaging against the rough degrees of freedom.

Another relevant work is [18]. In this paper, the authors sought to perform gradient based sampling on non-differentiable energy landscapes and proposed using a Moreau-Yosida regularization. This approach is related to one of the mechanisms that we propose in order to overcome roughness, though our potentials are smooth, but highly oscillatory.

### 1.2. Results on performance in the presence of roughness

In our investigation of (1.2), we also consider the separable form

$$V_{\epsilon,d}(x) = \sum_{i=1}^d \underbrace{v_0(x_i) + v_1(x_i, x_i/\epsilon)}_{\equiv v_\epsilon(x_i)}. \quad (1.13)$$

Again,  $v_0$  is trapping while  $v_1$  is uniformly bounded. Both  $v_0(x_i)$  and  $v_1(x_i, y_i)$  will be smooth functions. Our key observations and results are:

- (i) The performance of RWM for (1.2), as measured by MSD, is insensitive as  $\epsilon \rightarrow 0$ . This is a consequence of Theorem 1. Indeed, any method that uses  $\epsilon$ -independent proposals will be robust as  $\epsilon \rightarrow 0$  for potentials of type (1.2)
- (ii) An asymptotic analysis of MALA for (1.2) indicates that MALA's performance is degraded in the  $\epsilon \rightarrow 0$  limit. For  $d$  sufficiently large, we conclude that the optimal scaling is  $\sigma \propto \epsilon$ , so that  $\text{MSD}/n \propto \epsilon^2$ . Numerical experiments confirm this scaling, and it is consistent with prior analysis on potentials of type (1.13) in the  $n \rightarrow \infty$  limit.
- (iii) While this analysis of MALA does not hold in low dimension (*i.e.*,  $d = 1$ ), numerical experiments indicate that the optimal scaling is  $\sigma \propto \sqrt{\epsilon}$ , so that  $\text{MSD}/n \propto \epsilon$ . Thus, the collapse of MALA appears to be generic. An explicit example in  $n = 1$  is presented confirming the  $\sqrt{\epsilon}$  scaling.
- (iv) We formulate two alternative methods for potentials of type (1.2) that use large scale information contained in  $V_0$ . The first, Modified MALA, uses the proposals (at  $\beta = 1$ )

$$X_{k+1}^P = X_k - \frac{\sigma^2}{2} \nabla V_0(X_k) + \sigma \xi_{k+1}. \quad (1.14)$$

The latter is an MCMC Independence Sampler that uses proposals (at  $\beta = 1$ )

$$X_{k+1}^P = Y_{k+1} \sim e^{-V_0(x)} dx. \quad (1.15)$$

The  $Y_k$  samples can be obtained from standard MALA for  $V_0$ . Both of these methods are also insensitive to the roughness and outperform RWM. As both of these methods use  $\epsilon$ -independent proposals, Theorem 1 allows us to conclude they will also be robust in the  $\epsilon \rightarrow 0$  limit.

- (v) For potentials that do not admit an obvious decomposition like (1.2), we propose using local entropy approximation, [19, 20] to extract the large scale information needed for either the Modified MALA method or the independence sampler.

That the  $\epsilon \rightarrow 0$  limit might be problematic should not be surprising. Were we to numerically integrate  $\dot{x} = -V'_\epsilon(x)$ , we would immediately be confronted with the problem of stiffness. Stability of the explicit Euler method would require a time step  $\Delta t \lesssim \epsilon$ . For methods like RWM and MALA, the challenge of roughness is also hinted at (1.11). In the case of RWM,  $\mathcal{K}[v] = \mathbb{E}[|v'(X)|^2]$ . Thus, for potentials like (1.13),  $\mathcal{K}[v_\epsilon] \sim \epsilon^{-2}$ , driving the acceptance rate to zero for any fixed  $\ell$ ; we will further examine this below, in Section 2.

### 1.3. Outline

This work is organized as follows. In Section 2, we identify bound on the performance of RWM and other algorithms, and we consider the asymptotic behavior of MALA as  $\epsilon \rightarrow 0$ . In Section 3, we present alternative methods that are also robust to  $\epsilon \rightarrow 0$ . Numerical experiments are presented in 4, and we conclude with a discussion in Section 5

### Acknowledgements

GS was supported by US National Science Foundation Grant DMS-1818716, the work of PP was partially supported by DARPA project W911NF-15-2-0122. The authors thank UCLA IPAM for hosting them during the beginning of this project. The authors also thank M. Luskin, S. Osher, J. Mattingly, and N. Bou-Rabee for helpful discussions.

## 2. Bounds on performance and asymptotic analysis

In this section, we present results on the performance, as measured by the MSD (or  $\text{MSD}/n$ ), as defined in (1.7). For any MCMC method, let  $q(x \rightarrow y)$  denote the proposal kernel, and define

$$R(x, y) = V(x) - V(y) + \log \frac{q(y \rightarrow x)}{q(x \rightarrow y)}. \quad (2.1)$$

Consequently, the proposal  $X_n^p$  is accepted with probability  $F(R(X_n, X_n^p))$ . The two forms of  $F$  that we consider here are

$$\text{Metropolis: } F(r) = 1 \wedge e^r \quad (2.2a)$$

$$\text{Barker: } F(r) = (1 + e^{-r})^{-1} \quad (2.2b)$$

The reason for considering the Barker rule is that it allows us to compute derivatives of certain quantities, while having qualitatively similar behavior to the Metropolis rule.

### 2.1. Roughness independent bounds

For potentials of type (1.2), one can obtain  $\epsilon$ -independent upper and lower bounds on a variety of quantities. Indeed, by the boundedness assumption in the introduction, we are assured that

$$\text{osc } V_1 = \sup_x V_1(x, x/\epsilon) - \inf_x V_1(x, x/\epsilon) < \infty. \quad (2.3)$$

Our main result is the following:

**Theorem 1.** *Let  $V_\epsilon$  be a potential of type (1.2), and assume  $V_1$  has uniform in  $\epsilon$  bounded oscillation in the sense of (2.3). If the sampling strategy uses proposals  $q(x \rightarrow y)$  that are  $\epsilon$ -independent, then the performance, as measured by MSD, is  $\epsilon$ -independent and, in equilibrium,*

$$e^{-2 \text{osc } V_1} \mathbb{E}_{\mu_0} [|X_{k+1} - X_k|^2] \leq \text{MSD} \leq e^{2 \text{osc } V_1} \mathbb{E}_{\mu_0} [|X_{k+1} - X_k|^2]. \quad (2.4)$$

In (2.4),  $\mu_0(dx) \propto e^{-V_0(x)} dx$ .

To obtain this result, we first prove the following bounds on the distribution

**Lemma 2.** *Let  $V_\epsilon$  be a potential of type (1.2), and assume  $V_1$  has uniform in  $\epsilon$  bounded oscillation in the sense of (2.3). Then*

$$e^{-\text{osc } V_1} \mu_0(dx) \leq \mu(dx) \leq e^{\text{osc } V_1} \mu_0(dx) \quad (2.5)$$

PROOF. The proof of this follows from direct estimates on the densities. First,

$$Z^{-1} e^{-V(x)} \geq Z^{-1} e^{-V_0(x)} e^{-\sup V_1(x, x/\epsilon)}$$

while

$$Z = \int e^{-V(x)} dx \leq \underbrace{\int e^{-V_0(x)} dx}_{\equiv Z_0} e^{-\inf V_1(x, x/\epsilon)}$$

As a consequence, we have

**Corollary 3.** *Let  $V_\epsilon$  satisfy the same assumptions as in Lemma 2. Then for any non-negative observable,  $\mathcal{O}_\epsilon$ , which may depend on a small parameter  $\epsilon$ ,*

$$e^{-\text{osc } V_1} \mathbb{E}_{\mu_0} [\mathcal{O}_\epsilon(X)] \leq \mathbb{E}_\mu [\mathcal{O}_\epsilon(X)] \leq \mathbb{E}_{\mu_0} [\mathcal{O}_\epsilon(X)] e^{\text{osc } V_1}. \quad (2.6)$$

Consequently, the scaling of  $\mathbb{E}_\mu [\mathcal{O}_\epsilon(X)]$  as  $\epsilon \rightarrow 0$  is determined by the scaling of  $\mathcal{O}_\epsilon$ .

We now prove Theorem 1:

PROOF. Given any potential  $V$ , let  $\tilde{V}(x)$  be another potential, also bounded from below. Then

$$R(x, y) = \underbrace{(V(x) - \tilde{V}(x))}_{\Delta(x)} - \underbrace{(V(y) - \tilde{V}(y))}_{\Delta(y)} + \underbrace{\log \left( \frac{e^{-\tilde{V}(y)} q(y \rightarrow x)}{e^{-\tilde{V}(x)} q(x \rightarrow y)} \right)}_{\tilde{R}(x, y)} \quad (2.7)$$

If  $\text{osc } \Delta$  is bounded, then

$$\tilde{R}(x, y) + \text{osc } \Delta \geq R(x, y) \geq +\tilde{R}(x, y) - \text{osc } \Delta. \quad (2.8)$$

Consequently, for either choice of (2.2),

$$e^{\text{osc } \Delta} F(\tilde{R}(x, y)) \geq F(R(x, y)) \geq e^{-\text{osc } \Delta} F(\tilde{R}(x, y)). \quad (2.9)$$

For (1.2), we take  $\tilde{V} = V_0$ , so that  $\text{osc } \Delta = \text{osc } V_1$ , which we have assumed to be uniformly bounded in  $\epsilon$ . In this case, we let  $\tilde{R} = R_0$ , and  $R_0$  corresponds to the needed term for reversibility with respect to  $e^{-V_0(x)}$ , with proposals generated from  $q$ .

If the proposal,  $q(x \rightarrow y)$ , is also  $\epsilon$ -independent, then, for any  $X_0$ ,

$$\begin{aligned} \mathbb{E}[|X_1 - X_0|^2] &= \mathbb{E}[|X_1^P - X_0|^2 F(R(X_0, X_1^P))] \\ &\geq e^{-\text{osc } V_1} \mathbb{E}[|X_1^P - X_0|^2 F(R_0(X_0, X_1^P))] \end{aligned} \quad (2.10a)$$

$$\mathbb{E}[|X_1 - X_0|^2] \leq e^{\text{osc } V_1} \mathbb{E}[|X_1^P - X_0|^2 F(R_0(X_0, X_1^P))] \quad (2.10b)$$

In the preceding upper and lower bounds on  $\mathbb{E}[|X_1 - X_0|^2]$ , no  $\epsilon$  is present. If we are in stationarity,  $X_0 \sim \mu$ , and we can apply Lemma 2 to the upper and lower bounds in (2.10) to obtain (2.4).

Theorem 1 immediately applies to RWM, as it has an  $\epsilon$ -independent proposal. Consequently, for RWM,

$$\text{MSD} = \mathbb{E}_\mu[|X_{k+1} - X_k|^2] \sim \sigma^2.$$

In contrast, as MALA proposals include gradients of the potential, for potentials of the form (1.2), the theorem will not apply.

## 2.2. Asymptotic analysis of MALA

Next, we perform an asymptotic analysis of the performance of MALA. Without loss of generality, we take  $\beta = 1$ . For MALA we can write

$$R(x, y) = V(x) - V(y) - \frac{\sigma^2}{8} |\nabla V(x) + \nabla V(y)|^2 + \frac{\sigma}{2} \xi \cdot (\nabla V(x) + \nabla V(y)), \quad (2.11)$$

where  $y$  is the proposal generated from  $x$  by (1.4). We then define  $M(\sigma)$  to be the MSD obtained with  $\sigma$ , assuming stationarity,  $x \sim \mu$ , with the Barker rule, (2.2b). Thus, the optimal value of  $\sigma$  can be obtained by solving  $M'(\sigma) = 0$ . We calculate this derivative and argue via a dominant balance argument that at optimality and in sufficiently a high dimension,  $\sigma \sim \epsilon$ ; this is consistent with the numerical simulations in Section 4. In this scaling,  $\text{MSD} \lesssim \epsilon^2$ , so that the performance degrades to zero as  $\epsilon \rightarrow 0$ .

Proceeding with this strategy,

$$M(\sigma) = \int |x - y|^2 F(R(x, y; \sigma)) g(y; x, \sigma) dy \mu(dx) \quad (2.12)$$

where  $g$  is the Gaussian density of the normal distribution  $N(x - \frac{\sigma^2}{2} \nabla V(x), \sigma^2 I)$  and  $\mu(dx)$  is the Boltzmann distribution. Note that in (2.12) all of the  $\sigma$  dependence is in  $F$  and  $g$ . Differentiating  $M$  with respect to  $\sigma$  and setting the result to zero, we obtain:

$$0 = \frac{\sigma^2}{4} \underbrace{\mathbb{E} [|x - y|^2 F (F |\nabla V(x)|^2 + (1 - F) |\nabla V(y)|^2)]}_{\equiv A} + \sigma^2 n \underbrace{\mathbb{E} [|x - y|^2 F]}_{\equiv B} - \underbrace{\mathbb{E} [|x - y|^4 F]}_{\equiv C} \quad (2.13)$$

See Appendix A for details of this derivation. Consequently,

$$\sigma^2 = 2 \frac{\sqrt{(nB)^2 + AC} - nB}{A} = 2 \left\{ \frac{nB}{C} + \sqrt{\left( \frac{nB}{C} \right)^2 + \frac{A}{C}} \right\}^{-1}. \quad (2.14)$$

We interpret the expectations in  $A$ ,  $B$ , and  $C$  as over  $x$  and  $\xi$ , with  $y$  defined in terms of  $x$  and  $\xi$  through (1.4). No approximation or assumptions have yet been made.

For potentials of type (1.2), owing to Corollary 3, the scalings of  $A$ ,  $B$ , and  $C$  with  $\sigma$  and  $\epsilon$  will be determined by their integrands. We let  $f$  and  $\eta$  be characteristic values of  $F$  and  $|x_i - y_i|$ . Consequently,  $|x - y|^2 \sim n\eta^2$ . Both  $f$  and  $\eta$  are assumed to vary with  $\epsilon$ . Additionally,  $|\nabla V|^2 \sim n\epsilon^{-2}$ . For a sufficiently high dimension, the integrands of  $A$ ,  $B$ , and  $C$  are only weakly correlated through the acceptance probability  $F = F(R(X_k, X_{k+1}^P))$

$$B = \sum_{i=1}^n \mathbb{E} [|x_i - y_i|^2 F] \approx \sum_{i=1}^n \mathbb{E} [|x_i - y_i|^2] \mathbb{E}[F] \sim n\eta^2 f. \quad (2.15)$$

Analogously, in  $A$  and  $C$ , the majority of the terms are weakly correlated through  $F$ . Thus, we assume that:

$$A \sim n^2 \eta^2 f \epsilon^{-2}, \quad B \sim n\eta^2 f, \quad C \sim n^2 \eta^4 f, \quad (2.16)$$

are valid approximations. The decorrelation of the integrand terms was rigorously established in the  $n \rightarrow \infty$  limit in, for instance, [21] for potentials of type (1.13). We return to the high dimensional limit, below, in Section 2.3. Our numerical experiment show that  $n$  need not be that high, but there is deviation in low dimension. An explicit example is given below in Section 2.4.

We consider three different possible regimes to identify the optimal scaling, using (2.14), in order to verify the self-consistency of our asymptotic approximations. Letting  $\sigma/\epsilon = \tau$  the three regimes are:

**Regime I**  $\tau \rightarrow \infty$  In this first regime, as  $\tau \rightarrow \infty$  (i.e.,  $\sigma \gg \epsilon$ ),

$$\epsilon^2 \sigma^{-4} |x - y|^2 = \underbrace{\frac{1}{4} \epsilon^2 |\nabla V(x)|^2}_{\sim n} - \underbrace{\epsilon^2 \sigma^{-1} \nabla V(x) \cdot \xi}_{\sim n\tau^{-1}} + \underbrace{\epsilon^2 \sigma^{-2} |\xi|^2}_{\sim n\tau^{-2}} = n \cdot O(1). \quad (2.17)$$

Consequently,  $\epsilon^2 \sigma^{-4} \eta^2 = O(1)$  in this regime. Substituting back in,  $(nB)^2/(AC) \sim \tau^{-4} \ll 1$ . Substituting this into (2.14):

$$\sigma^2 = 2\sqrt{\frac{C}{A}} + \text{higher order terms} \sim \epsilon\eta \sim \sigma^2 \quad (2.18)$$

In the last estimate we have used that  $\epsilon^2 \sigma^{-4} \eta^2 = O(1)$ . Thus,  $\eta^2 \sim \sigma^4 \epsilon^{-2}$  is self-consistent when  $\tau \rightarrow \infty$ .

**Regime II**  $\tau \rightarrow 0$  In this second regime we observe that as  $\tau \rightarrow 0$  (*i.e.*  $\sigma \ll \epsilon$ )

$$\epsilon^{-2} |x - y|^2 = \underbrace{\frac{1}{4} \sigma^2 |\nabla V(x)|^2}_{\sim n\tau^2} - \underbrace{\sigma \nabla V(x) \cdot \xi}_{\sim n\tau} + \underbrace{|\xi|^2}_{\sim n} = n \cdot O(1). \quad (2.19)$$

Consequently,  $\sigma^{-2} \eta^2 = O(1)$  in this regime. Substituting back in,  $(nB)^2/(AC) \sim \tau^{-2} \gg 1$ , and subsequently into (2.14):

$$\sigma^2 = \frac{C}{dB} + \text{higher order terms} \sim \eta^2 \sim \sigma^2. \quad (2.20)$$

Thus, in this regime,  $\eta^2 \sim \sigma^2$  is self-consistent when  $\tau \rightarrow 0$ .

**Regime III**  $\tau = O(1)$  Finally, in this case where  $\sigma \sim \epsilon$  we have

$$\epsilon^{-2} |x - y|^2 = \underbrace{\frac{1}{4} \sigma^4 \epsilon^{-2} |\nabla V(x)|^2}_{\sim n\tau^4} - \underbrace{\sigma^3 \epsilon^{-2} \nabla V(x) \cdot \xi}_{\sim n\tau^3} + \underbrace{\sigma^2 \epsilon^{-2} |\xi|^2}_{\sim n\tau^2} = n \cdot O(1). \quad (2.21)$$

Consequently,  $(nB)^2/(AC) \sim \tau^{-2} = O(1)$ , and in (2.14), and  $\sigma \sim \epsilon$  is self-consistent.

We now estimate the MSD in these three regimes to determine which is optimal. This will require estimating  $f$  through (2.11) as  $\epsilon \rightarrow 0$ . In all three regimes we estimate the latter two terms of  $R$  as

$$\frac{\sigma^2}{8} |\nabla V(x) + \nabla V(y)|^2 \sim n\tau^2, \quad \frac{\sigma}{2} \xi \cdot (\nabla V(x) + \nabla V(y)) \sim n\tau.$$

For Regimes II and III,  $\eta \lesssim \epsilon$ , so that  $V(x) - V(y) = O(1)$ . In both Regimes II and III,  $R = O(1)$  and  $f = O(1)$  too.

For Regime I, in principle,  $\eta \sim \epsilon\tau^2$  could grow as  $\epsilon \rightarrow 0$  and  $\tau \rightarrow \infty$ , and  $V(x) - V(y)$  could be quite large in magnitude. In this case, we use that  $V$  is bounded from below, so that  $V(x) - V(y) \leq V(x) - V_{\min} = O(1)$ . Consequently,  $R \lesssim -Kn\tau^2$ , and  $f \lesssim e^{-Kn\tau^2}$ , for some constant  $K > 0$ , independent of  $\epsilon$ ,  $n$ , and  $\tau$ .

Summarizing,

$$\text{MSD } /n \sim \eta^2 f, \quad \begin{cases} \eta^2 f \lesssim \epsilon\tau^2 e^{-Kn\tau^2} & \text{Regime I } \tau \rightarrow \infty, \\ \eta^2 f \sim \epsilon^2 \tau^2 & \text{Regime II } \tau \rightarrow 0, \\ \eta^2 f \sim \epsilon^2 & \text{Regime III } \tau = O(1). \end{cases} \quad (2.22)$$

This suggests that the best performance is found in Regime III. To make a more precise assessment we further assume

$$\tau \sim \epsilon^\gamma, \quad \begin{cases} \gamma < 0 & \text{Regime I,} \\ \gamma > 0 & \text{Regime II,} \\ \gamma = 0 & \text{Regime III.} \end{cases} \quad (2.23)$$

Under this power law assumption

$$\begin{cases} \text{MSD}/n \lesssim \epsilon^{1+2\gamma} e^{-Kn\epsilon^\gamma} & \text{Regime I,} \\ \text{MSD}/n \sim \epsilon^{2+2\gamma} & \text{Regime II,} \\ \text{MSD}/n \sim \epsilon^2 & \text{Regime III.} \end{cases} \quad (2.24)$$

Hence Regime I vanishes exponentially fast with  $\epsilon$ , while Regime II vanishes faster than quadratic. Regime III only vanishes quadratically, yielding the best performance. Thus, the optimal choice is Regime III where  $\sigma \sim \epsilon$ . As noted, this assumes that the dimension is sufficiently high that the coordinates approximately decouple and (2.16) holds.

### 2.3. Insights from the high dimensional limit

Recall from the introduction that for separable distributions like (1.6), as  $n \rightarrow \infty$ , the MSD per degree of freedom is given by (1.8). Using (1.11) to find the optimal  $\ell$ , from which we can infer the optimal  $\sigma^2$ . This in turn gives us the scaling of the  $\text{MSD}/n$ , via (1.8). After changing variables to  $\lambda = -\ell^{1/I} \sqrt{\mathcal{K}[v]}/2$ , and optimizing in this transformed coordinate, one can deduce that the optimal  $\ell^2 \sim \mathcal{K}^{-I}$ . Consequently, for potentials like (1.13), the optimal scaling, as  $n \rightarrow \infty$ , is  $\sigma^2 \sim (n\mathcal{K})^{-I}$  and

- For RWM,  $I = 1$  and  $\mathcal{K}[v_\epsilon] = \mathbb{E}_\mu[(v'_\epsilon)^2]$ , so that  $\sigma^2 \sim \epsilon^2/n$ ;
- For MALA,  $I = 1/3$  and  $\mathcal{K}[v_\epsilon] = \mathbb{E}_\mu[5(v''_\epsilon)^2 + 3(v''_\epsilon)^3]/48 \sim \epsilon^{-6}$  so that  $\sigma^2 \sim \epsilon^2/n^{1/3}$ .

In this limit, both RWM and MALA are crippled as  $\epsilon \rightarrow 0$ . Note that this does not contradict the analysis of Section 2.1. There, in the separable case, our lower bound would have the prefactor  $e^{-n \text{osc } v_1}$ , which vanishes far more rapidly than the  $\epsilon^2/n$  we have here. This also shows consistency with our asymptotic analysis in Section 2.2 as we recover  $\sigma \propto \epsilon$  as  $n \rightarrow \infty$ .

### 2.4. Scaling in dimension $n = 1$

We consider the question of sampling from the distribution associated with  $V(x) = \frac{k}{2}x^2$  in  $n = 1$ , using MALA. While this may seem odd, as this corresponds to a Gaussian distribution, it reveals a distinct scaling in low dimensions. It can be interpreted as the necessary scaling to efficiently sampling individual modes of the highly multi-modal landscape in Figure 1(b), or alternatively, as the analog of the stiff differential equation problem  $\dot{x} = -\lambda x$ ,  $\lambda \gg 1$ . We will

ultimately consider the case of the harmonic potential with  $k = 1/\epsilon$  and examine the  $\epsilon \rightarrow 0$  limit.

In this case,

$$X_{j+1}^p = X_j - \frac{\sigma^2}{2} k X_j + \sigma \xi_{j+1}, \quad (2.25)$$

and the term in the accept/reject rule is

$$R(x, y) = \frac{\sigma^2 k^2}{8} (x^2 - y^2). \quad (2.26)$$

With the aid of a computer algebra system (see, also, Appendix B) we conclude

$$\begin{aligned} \text{MSD} &= \frac{1}{k} \frac{2\delta}{\pi(4 + \delta(-2 + \delta))} \left\{ (8 + \delta^3) \arctan \left( \sqrt{\frac{8}{\delta^3}} \right) - 2\sqrt{2}\delta^{3/2} \right\} \\ &= k^{-1} m(\delta). \end{aligned} \quad (2.27)$$

The  $m(\delta)$  function has a single maximum (see Figure B.11), and the maximum value is achieved at  $\delta_* = 1.27797$ , and  $m(\delta_*) = 1.8494$ . Thus, the optimal scaling for the time step is

$$\sigma = \sqrt{\frac{2\delta_*}{k}} \approx \frac{1.59873}{\sqrt{k}}.$$

Consequently, if  $k = 1/\epsilon$ ,  $\sigma \propto \sqrt{\epsilon}$ , which is indeed different from the scaling found in Section 2.2. We note that this optimal choice is smaller than the Euler-Maruyama stability threshold which requires  $\sigma \leq 2\sqrt{\epsilon}$ .

### 3. Alternative algorithms for rough landscapes

Having concluded that there are impediments to MALA for sampling on rough landscapes, but desiring a method that may perform better than RWM, we propose two methods here. Both these methods require a smoothed version of the potential which may not be accessible. Indeed, as the potential of interest is unlikely to admit a simple decomposition like (1.2), we also propose a method for approximating a smoothed landscape.

#### 3.1. Modified MALA

The first method, which we call Modified MALA, involves generating proposals from an auxiliary potential,  $U$ . The algorithm generates the proposals

$$X_{k+1}^p = X_k - \frac{\sigma^2}{2} \nabla U(X_k) + \sigma \xi_{k+1}, \quad (3.1)$$

and  $R(x, y)$  is modified to be

$$R(x, y) = V(x) - V(y) - \frac{1}{2\sigma^2} |x - y + \nabla U(y) \frac{\sigma^2}{2}|^2 + \frac{1}{2\sigma^2} |y - x + \nabla U(x) \frac{\sigma^2}{2}|^2. \quad (3.2)$$

If the scale separation in (1.2) holds, we might take  $U = V_0$  to get (1.14). Since the proposal is  $\epsilon$ -independent, Theorem 1 applies to this method.

### 3.2. Coupled independence sampling

The second method we propose is to generate auxiliary samples,  $Y_k$ , from another distribution  $\propto e^{-U(x)}dx$ , and perform independence sampling against  $\mu(dx) \propto e^{-V(x)}dx$ . More explicitly,

$$\Delta(x) = V(x) - U(x), \quad R(x, y) = \Delta(x) - \Delta(y) \quad (3.3a)$$

$$X_{k+1} = \begin{cases} Y_{k+1}, & \text{with probability } F(R(X_k, Y_{k+1})), \\ X_k, & \text{otherwise.} \end{cases} \quad (3.3b)$$

This amounts to MCMC importance sampling, and we should thus expect the best performance when  $\Delta$  is small. Indeed, if our assumptions about (1.2) hold, then we would take  $U = V_0$  giving us (1.15). Theorem 1 again applies to this method.

The question of how to generate the  $Y_k$  samples remains. Here, we propose to use MALA for samples of  $e^{-U}$  on the fly, taking  $U = V_0$  from (1.2) in the case that such a decomposition is available. Thus, the  $Y_k$  are no longer independent samples.

### 3.3. Finding smoothed landscapes

A question that remains is what to do when (1.2) fails to hold. One option is to use physical intuition about the problem to identify a potential  $U(x)$  that has suitable properties. More systematically, we can use the local entropy approach formulated in [19, 20], or, equivalently the Moreau-Yosida approximation to estimate a smoothed version of  $V(x)$ .

Given  $\gamma > 0$ , we define  $V_\gamma$  as

$$V_\gamma(x) = -\beta^{-1} \log N(0, \gamma\beta^{-1}I) * e^{-\beta V(x)}, \quad (3.4)$$

which corresponds to a Gaussian filter of the Boltzmann distribution. The associated gradient is then

$$\nabla V_\gamma(x) = \gamma^{-1} \int_{\mathbb{R}^d} (x - y) \rho_\infty(y \mid x) dy = \gamma^{-1} (x - \mathbb{E}^{\rho_\infty(\cdot \mid x)}[Y]). \quad (3.5)$$

The density,  $\rho_\infty(y \mid x)$ , can be defined by first introducing

$$U_\gamma(y \mid x) = V(y) + \frac{1}{2\gamma} |x - y|^2, \quad (3.6)$$

so that

$$\rho_\infty(y \mid x) \propto e^{-\beta U_\gamma(y \mid x)}.$$

The potential  $V_\gamma$  could be estimated with the simple Monte Carlo scheme

$$V_\gamma(x) \approx -\beta^{-1} \log \left( \frac{1}{N_s} \sum_{j=1}^{N_s} e^{-\beta V(x + Y^{(j)})} \right), \quad Y^{(j)} \sim N(0, \gamma\beta^{-1}I). \quad (3.7)$$

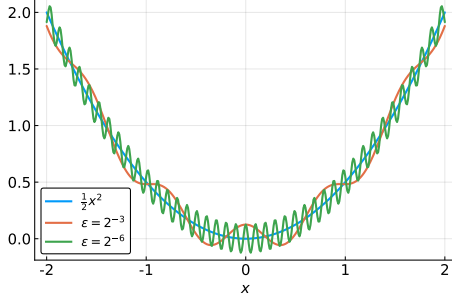


Figure 3: Harmonic potential (4.1) with an additive rough term (color online).

Likewise, (3.5) could be estimated by integrating the auxiliary diffusion

$$dY_t = -\nabla U_\gamma(Y_t \mid x)dt + \sqrt{2\beta^{-1}}dW_t^y \quad (3.8)$$

If  $V$  is assumed to grow at infinity, then for sufficiently small  $\gamma$ ,  $U_\gamma(y \mid x)$  will be convex about  $y = x$ , and (3.8) to converge to equilibrium exponentially fast. The potential  $\nabla V_\gamma$  can then be estimated by Monte Carlo

$$\nabla V_\gamma(x) \approx \frac{1}{N_s} \sum_{j=1}^{N_s} \gamma^{-1}(x - Y^{(j)}), \quad (3.9)$$

where each  $Y^{(j)} \sim \rho_\infty(\cdot \mid x)$ . Of course,  $Y^{(j)}$  must now be appropriately sampled. Running short i.i.d. samples of (3.8) using, for instance, MALA, the algorithm introduces three additional numerical parameters:  $N_s$ , the number of samples;  $\delta t$ , the fine scale time step; and  $N_{\delta t}$ , the number of fine scale time steps. We must also specify initial conditions.

With estimates of  $V_\gamma$  and  $\nabla V_\gamma$ , we then use them as the smoothed landscapes in our coupled independence sampler scheme or our Modified MALA scheme.

## 4. Numerical experiments

In this section we demonstrate, numerically, how roughness can impede MALA, and how RWM, along with the methods discussed in Section 3, can resist the roughness. In these computational examples, we use the Metropolis rule, (2.2a).

### 4.1. Rough harmonic potential

As a first example, we consider a potential of type (1.13), with

$$v_\epsilon(x_i) = \frac{1}{2}x_i^2 + \frac{1}{8} \cos(x_i/\epsilon). \quad (4.1)$$

This is pictured in Figure 3 at various values of  $\epsilon$ .

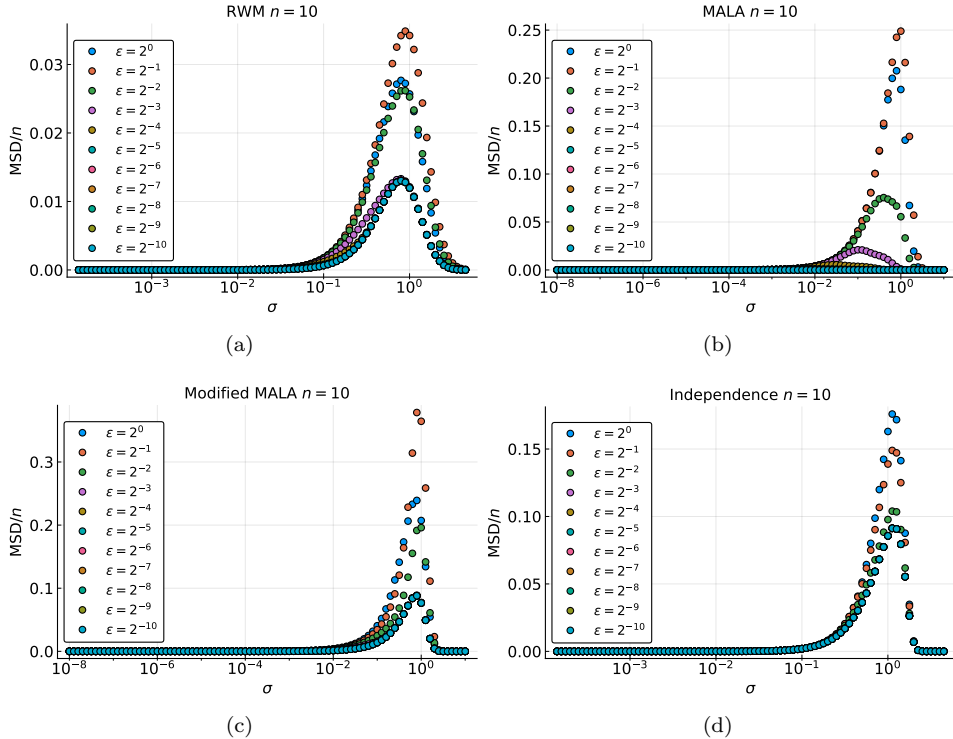


Figure 4: Example computations of the MSD for (4.1) for a variety of  $\sigma$  and  $\epsilon$  values. The empirical maximum, for each  $\sigma$ ,  $\epsilon$  pair is interpreted to be the optimal choice (color online).

We explore this potential by varying both  $\epsilon$  and the dimension  $n$ . *A priori*, we do not know the optimal value of  $\sigma$  for each  $\epsilon$  and  $n$  pair, for each algorithm. Thus, we examine a range of  $\sigma$  values, run long trajectories for each, and then empirically estimate the one with the maximum MSD. See Figure 4 for examples of such a computation. In this way we are able to compare performance across methods. In these experiments inverse temperature is restored to the value  $\beta = 5$  and  $10^8$  iterations are performed in each run.

Having estimated the optimal  $\sigma$ , we can then compare performance between the algorithms, as a function of  $\epsilon$  and  $n$ . This is shown in Figure 5. This reveals that, as predicted in Section 2,  $\sigma \propto \epsilon$  for MALA, provided  $n$  is large enough. Furthermore, at the optimal value of  $\sigma$ , while MALA will have a comparatively high acceptance rate, the mixing, as measured by the MSD, is impeded because of the smallness of  $\sigma$ . Also note that the mean acceptance rates across a range of  $\epsilon$  and  $n$  deviate from the idealized  $n \rightarrow \infty$  RWM and MALA values.

Since RWM, Modified MALA, and the Independence sampler are all robust to  $\epsilon \rightarrow 0$ , we examined amplification in performance at different  $\epsilon$  and  $n$ , as

Table 1: Ratios of the MSD at optimal  $\sigma$  for Modified MALA and Independence sampler to the RWM for the rough harmonic landscape, (4.1). As  $\epsilon \rightarrow 0$ , the amplification in performance saturates, but increases with dimension. The Independence sampling method appears to give better performance in moderate to high dimension.

(a) Modified MALA Sampler					
$\epsilon$	$n = 1$	$n = 10$	$n = 20$	$n = 50$	$n = 100$
$2^{-5}$	2.43	6.73	9.57	15.98	3.86
$2^{-6}$	2.43	6.74	9.61	15.71	13.59
$2^{-7}$	2.43	6.74	9.64	15.41	21.85
$2^{-8}$	2.43	6.74	9.57	15.65	21.29
$2^{-9}$	2.43	6.75	9.58	15.75	21.00
$2^{-10}$	2.43	6.75	9.60	15.27	24.25

(b) Independence Sampler					
$\epsilon$	$n = 1$	$n = 10$	$n = 20$	$n = 50$	$n = 100$
$2^{-5}$	2.07	6.99	12.99	44.16	38.60
$2^{-6}$	2.07	6.99	13.02	42.84	157.52
$2^{-7}$	2.07	6.99	13.05	43.78	205.66
$2^{-8}$	2.07	6.98	12.99	44.06	221.49
$2^{-9}$	2.07	6.99	12.98	43.87	212.06
$2^{-10}$	2.07	7.00	13.01	43.12	230.18

measured by

$$\text{Performance Amplification} = \frac{\text{Optimal MSD for Alternative Method}}{\text{Optimal MSD for RWM}} \quad (4.2)$$

This is shown in Table 1. The alternative methods always beat RWM, and, there is greater improvement in higher dimension, though the performance improvement saturates as  $\epsilon \rightarrow 0$ . The independence method typically outperforms the Modified MALA method.

#### 4.2. Rough double well potential

We repeat the experiment from Section 4.1 for a more challenging problem of sampling from the distribution given by the potential

$$v_\epsilon(x_i) = (x_i^2 - 1)^2 + \frac{1}{8} \cos(x_i/\epsilon), \quad (4.3)$$

with parameters otherwise the same as in the harmonic case. Results here are shown in Figure 6 and Table 2. These are consistent with the experiments for the harmonic potential.

Furthermore, in Figure 7, we repeat the experiment from Figure 2 with  $n = 1$ , but for the Modified MALA and the Independence sampling schemes. Computing at  $\sigma = 1$ , we see better mixing than in Figure 2, for the same rough energy landscape.

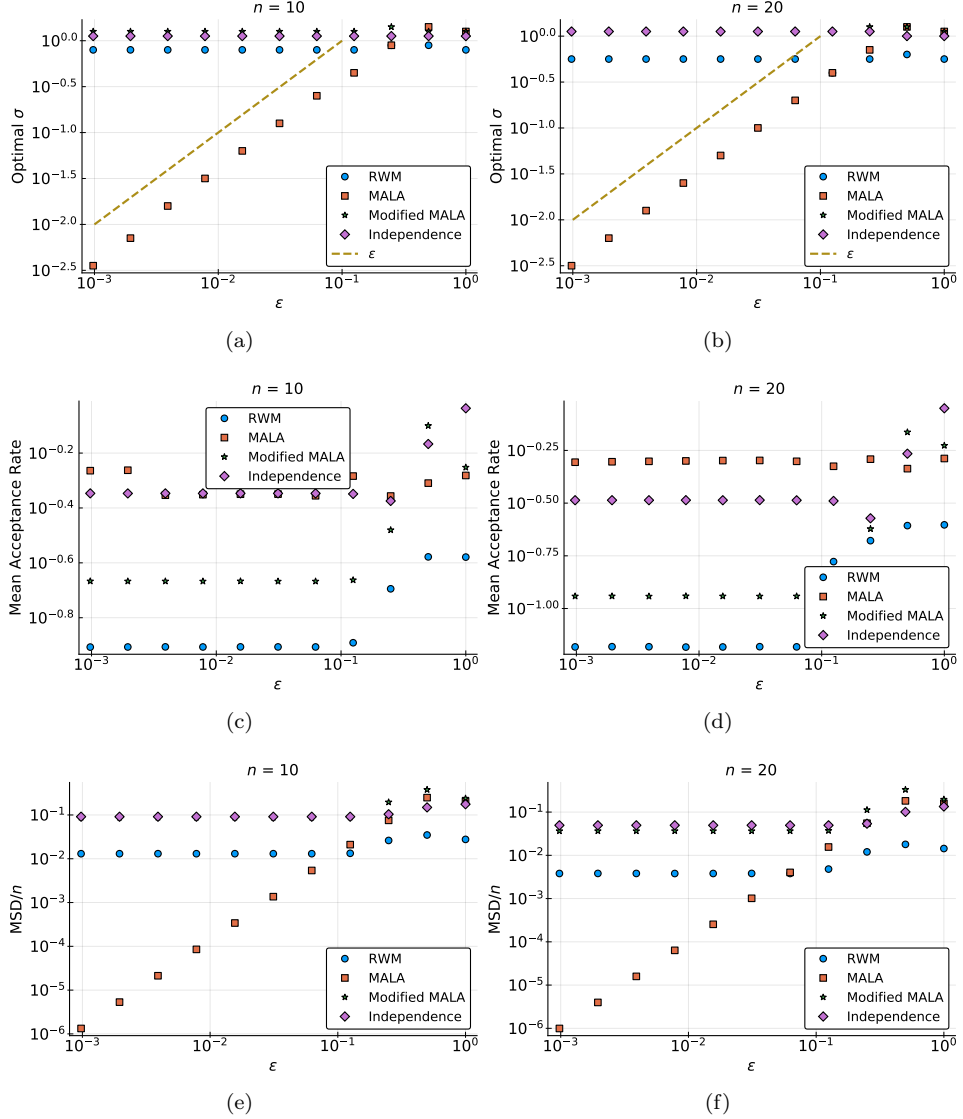


Figure 5: Comparison of performance for (4.1) in different dimensions for a range of  $\epsilon$ . Observe that the optimal  $\sigma \propto \epsilon$ , as predicted. Also note that while MALA maintains a comparatively higher acceptance rate, because its step size is shrinking, the mixing rate, as measured by the MSD vanishes with  $\epsilon$  (color online).

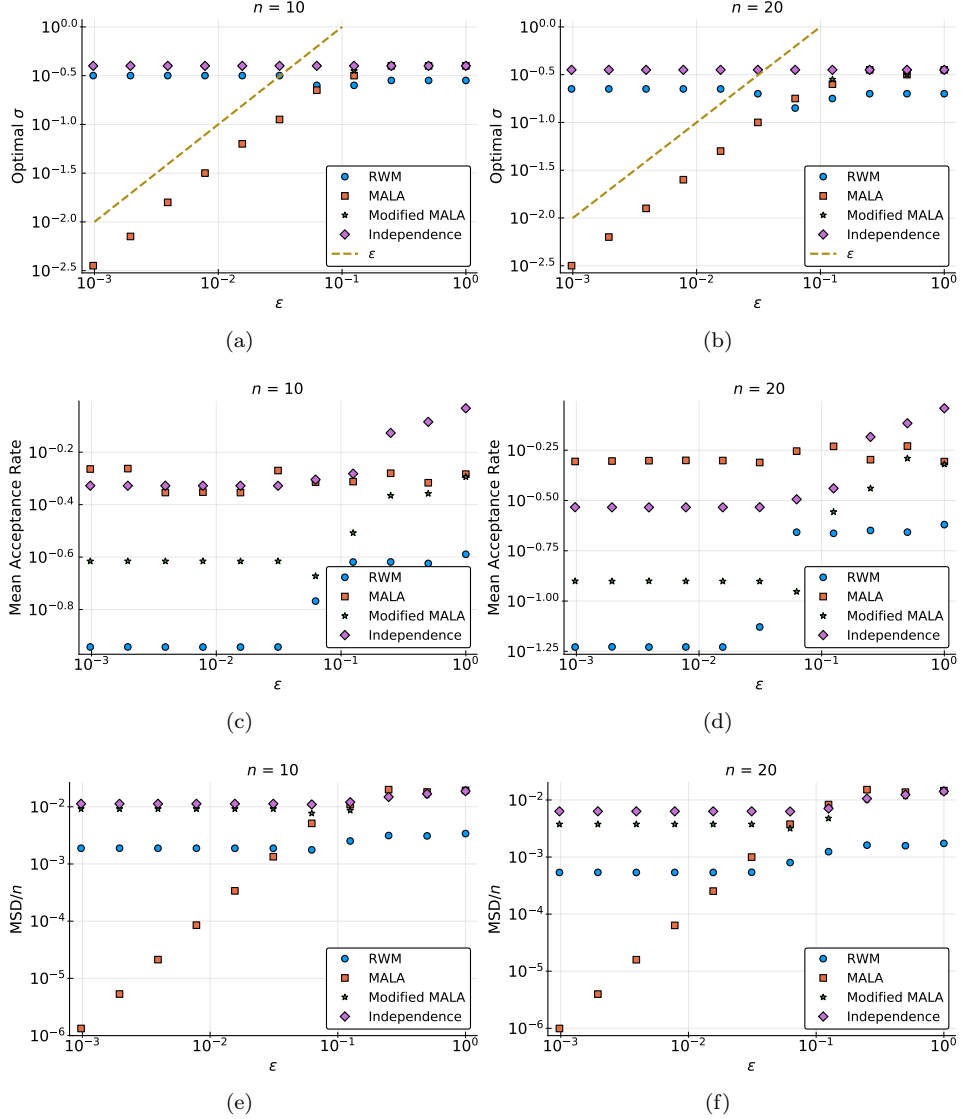


Figure 6: Comparison of performance for (4.3) in different dimensions for a range of  $\epsilon$ . Observe that the optimal  $\sigma \propto \epsilon$ , as predicted. Also note that while MALA maintains a comparatively higher acceptance rate, because its step size is shrinking, the mixing rate, as measured by the MSD vanishes with  $\epsilon$  (color online).

Table 2: Ratios of the MSD at optimal  $\sigma$  for Modified MALA and Independence sampler to the RWM for the rough double well landscape, (4.3). As  $\epsilon \rightarrow 0$ , the amplification in performance saturates, but increases with dimension. The Independence sampling method appears to give better performance in moderate to high dimension. In contrast to the harmonic potential, the  $n = 100$  results are somewhat less well converged here, though they still suggest improvement.

(a) Modified MALA Sampler

$\epsilon$	$n = 1$	$n = 10$	$n = 20$	$n = 50$	$n = 100$
$2^{-5}$	0.31	4.89	6.93	3.82	1.22
$2^{-6}$	0.30	4.89	6.98	11.66	1.87
$2^{-7}$	0.29	4.89	6.98	11.62	7.38
$2^{-8}$	0.29	4.89	7.00	11.46	15.77
$2^{-9}$	0.29	4.89	6.96	11.49	18.56
$2^{-10}$	0.29	4.89	6.99	11.63	18.43

(b) Independence Sampler

$\epsilon$	$n = 1$	$n = 10$	$n = 20$	$n = 50$	$n = 100$
$2^{-5}$	0.31	5.99	11.70	15.15	8.55
$2^{-6}$	0.31	5.99	11.77	45.86	28.79
$2^{-7}$	0.31	5.99	11.76	45.54	100.78
$2^{-8}$	0.31	5.99	11.77	46.11	221.20
$2^{-9}$	0.31	5.98	11.75	45.65	332.74
$2^{-10}$	0.31	5.99	11.78	47.07	309.31

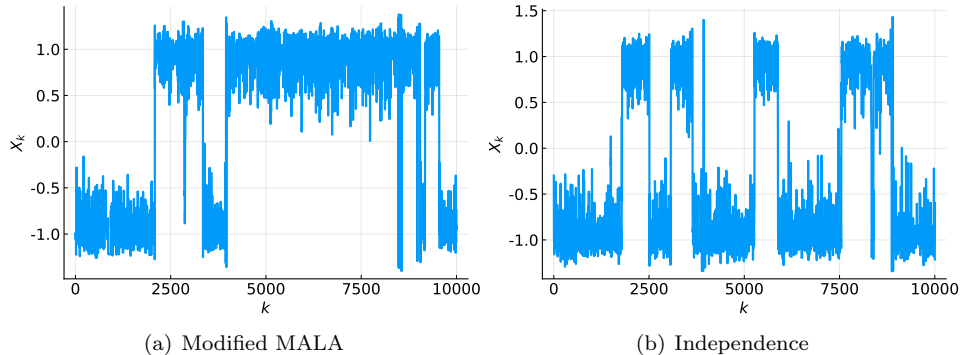


Figure 7: Sample paths corresponding to the energy landscapes in Figure 1(b). These were generated using MALA with  $\sigma = 1$ . Compare with standard MALA sampling in Figure 2(b) (color online).

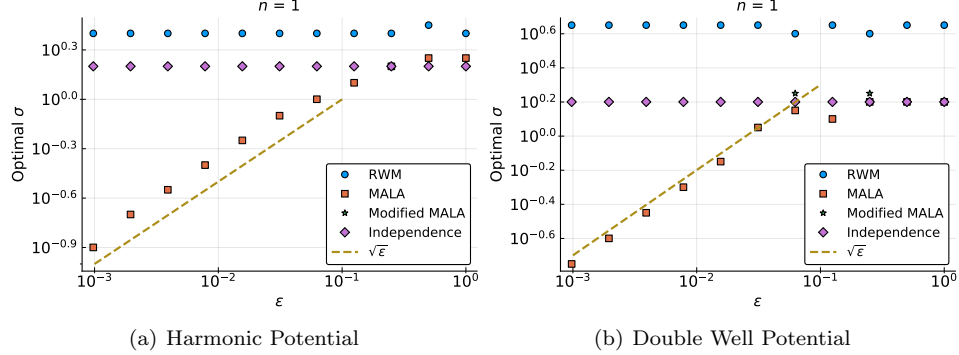


Figure 8: Optimal  $\sigma$  values for the rough harmonic and double well potentials in  $n = 1$ . In contrast to results in higher dimension (see Figures 5 and 6), for MALA,  $\sigma \propto \sqrt{\epsilon}$  for  $n = 1$ .

#### 4.3. Results in dimension $n = 1$

We briefly consider the behavior in dimension one for the harmonic potential and the double well. In both cases, as shown in Figure 8, the optimal  $\sigma \propto \sqrt{\epsilon}$ , not  $\sigma \propto \epsilon$ . Thus, while the performance of MALA will also degrade in  $n = 1$ , a different scaling appears here. As discussed in Section 2.2, it should not be too surprising that there is deviation here, as the weak correlation approximation will not hold in  $n = 1$ . This is consistent with the analysis of Section 2.4.

#### 4.4. Local entropy approximations

We briefly consider the possibility of using local entropy, introduced in Section 3.3 with (3.4) and (3.5). This approach may be of use in problems where no straightforward scale separation, of the sort found in (1.2), is present in the energy landscape. As motivation we consider the potential in dimension one

$$V(x) = \underbrace{(x^2 - 1)^2}_{V_0(x)} + \sum_{j=1}^M c_j \cos(k_j x), \quad (4.4)$$

where the  $c_j$  and  $k_j$  are random, from a particular distribution. Indeed, taking  $M = 10$  and  $c_j \sim U(-.1, .1)$ ,  $\log(k_j) \sim U(10^1, 10^3)$ , we obtain the landscape shown in Figure 9, along with the leading contribution,  $V_0$ , and  $V_\gamma$  obtained through a numerical quadrature at  $\beta = 5$  and  $\gamma = 0.05$ . Clearly, the local entropy approximation eliminates the fine scale roughness found in the original potential.

In general, Monte Carlo approximations of  $V_\gamma$  and  $\nabla V_\gamma$  will be needed, as a quadrature will be impractical in high dimension. An example of this is shown in Figure 10. In Figure 10(a), we compare  $V_0$ ,  $V_\gamma$  and a Monte Carlo estimate of  $V_\gamma$  computed using (3.7) with  $N_s = 10^2$ .

In Figure 10(b), we compare  $\nabla V_0$ ,  $\nabla V_\gamma$ , and a Monte carlo estimate of  $V_\gamma$ , computed using (3.9). In this latter figure, we take  $N_s = 10^4$ , and each

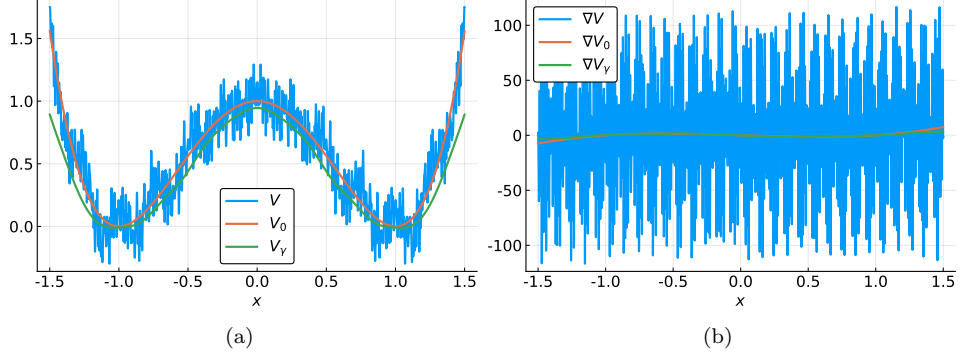


Figure 9: A particular realization of the energy landscape given by (4.4), along with its leading order, long range, component  $V_0(x) = (x^2 - 1)^2$ , and the local entropy approximation,  $V_\gamma$ , computed using (3.4) with  $\beta = 5$  and  $\gamma = 0.05$ .

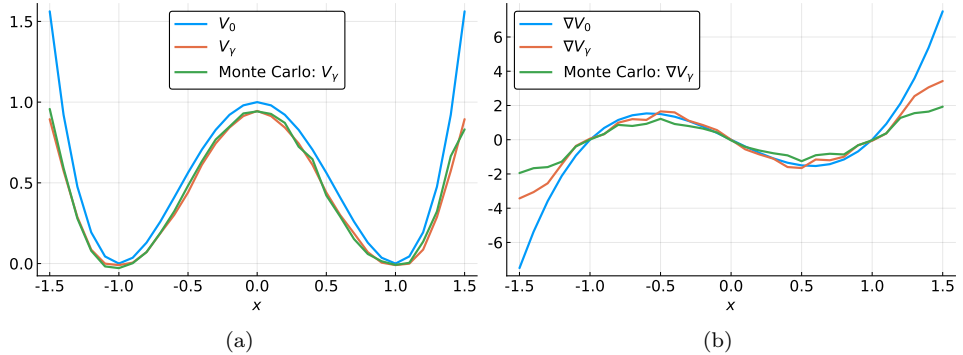


Figure 10: Monte Carlo estimates of  $V_\gamma$  and  $\nabla V_\gamma$  for the landscapes in Figure 9.

sample is obtained by taking  $N_{\delta t} = 4$  time steps with  $\delta t = 1$  in a variant of MALA that exactly linearly integrates the Ornstein-Uhlenbeck component of (3.8). Obviously, there are many options for how Monte Carlo estimates of  $V_\gamma$  and  $\nabla V_\gamma$  can be obtained. We will return to this in the discussion.

## 5. Discussion

We have examined a class of rough energy landscapes where the performance of MALA can be driven to zero, even in a finite dimension, at the optimally scaled  $\sigma$ . This defect of the scheme is suggested by asymptotic scaling and numerical experiments, where, for  $n$  sufficiently large, the optimal scaling is  $\sigma \propto \epsilon$ . In contrast, in a low dimension, such as  $n = 1$ , the scaling appears to be  $\sigma \propto \sqrt{\epsilon}$ . A fully rigorous basis for these scaling relations in a finite dimension remains an open problem. It would also be of interest to investigate different regimes when  $n \rightarrow \infty$  and  $\epsilon \rightarrow 0$ , simultaneously.

On the other hand, we have demonstrated that RWM along with the Modified MALA and the MCMC independence sampler are insensitive to the roughness of the landscape. While modified MALA and the MCMC independence sampler require a smoothed energy landscape for proposals, RWM is a viable option without additional information. Indeed, Theorem 1 tells us that for rough energy landscapes like (1.2), with roughness bounded uniformly in  $\epsilon$ , if the proposal of the MCMC scheme is  $\epsilon$ -independent, then the performance will be insensitive to  $\epsilon$ .

Smoothed energy landscapes might be available through a known decomposition like (1.2). We conjecture, that the optimal choice of approximate landscapes for potentials like (1.2) corresponds to the homogenized energy landscapes discussed in [3–5]. Unfortunately, computing such smoothed energies requires solving an elliptic PDE in a space of the same dimension as the considered state space; a Monte Carlo estimator of the solution may partially overcome this difficulty. Alternatively, physical knowledge of the system may motivate some choice for a surrogate smoothed landscape.

When these options are not available, the local entropy approximation is another possibility. The challenge to using local entropy, which we do not further develop here, is that unless the problem is in a very low dimension, auxiliary sampling algorithms must be formulated and tuned to first estimate  $V_\gamma$  and  $\nabla V_\gamma$ . This task would involve determining a sample size, a sampling strategy, and some form of parallelization in order to outperform simpler alternatives like RWM.

Finally, the weakness of MALA in the presence of roughness can be seen as the MCMC manifestation of stiffness. We conjecture that it is a generic problem in gradient based MCMC methods, including HMC. Indeed, the magnitude of  $\nabla V$  in HMC will constrain the time step of, for instance, the Verlet method used in the Hamiltonian flow subroutine. Thus, the number of force calls per HMC step will tend to increase with roughness degrading the overall performance. An investigation of HMC, is another outstanding problem.

## References

- [1] E. Pollak, A. Auerbach, P. Talkner, Observations on Rate Theory for Rugged Energy Landscapes, *Biophysical Journal* 95 (2008) 4258–4265.
- [2] M. Hu, J.-D. Bao, Diffusion crossing over a barrier in a random rough metastable potential, *Physical Review E* 97 (2018) 062143.
- [3] A. Duncan, S. Kalliadasis, G. Pavliotis, M. Pradas, Noise-induced transitions in rugged energy landscapes, *Physical Review E* 94 (3) (2016) 032107.
- [4] G. B. Arous, H. Owhadi, Multiscale homogenization with bounded ratios and anomalous slow diffusion, *Communications on Pure and Applied Mathematics* 56 (1) (2003) 80–113.
- [5] H. Owhadi, Anomalous slow diffusion from perpetual homogenization, *The Annals of Probability* 31 (4) (2003) 1935–1969.
- [6] G. O. Roberts, A. Gelman, W. R. Gilks, Weak convergence and optimal scaling of random walk metropolis algorithms, *The Annals of Applied Probability* 7 (1) (1997) 110–120.
- [7] G. O. Roberts, J. S. Rosenthal, Optimal scaling of discrete approximations to langevin diffusions, *Journal of the Royal Statistical Society: Series B (Statistical Methodology)* 60 (1) (1998) 255–268.
- [8] A. Beskos, G. Roberts, A. Stuart, Optimal scalings for local metropolis–hastings chains on nonproduct targets in high dimensions, *The Annals of Applied Probability* 19 (3) (2009) 863–898.
- [9] A. Beskos, G. Roberts, A. Thiery, N. Pillai, Asymptotic analysis of the random-walk metropolis algorithm on ridged densities, *Annals of Probability*.
- [10] J. Kuntz, M. Ottobre, A. M. Stuart, Diffusion limit for the random walk metropolis algorithm out of stationarity (2014). [arXiv:arXiv:1405.4896](https://arxiv.org/abs/1405.4896).
- [11] J. Kuntz, M. Ottobre, A. M. Stuart, Non-stationary phase of the mala algorithm, *Stochastics and Partial Differential Equations: Analysis and Computations* 6 (3) (2018) 446–499.
- [12] J. Kuntz, M. Ottobre, A. M. Stuart, Non-stationary phase of the MALA algorithm, *Stochastics and Partial Differential Equations: Analysis and Computations* (2018) 1–54.
- [13] M. Ottobre, N. S. Pillai, F. J. Pinski, A. M. Stuart, et al., A function space hmc algorithm with second order langevin diffusion limit, *Bernoulli* 22 (1) (2016) 60–106.
- [14] N. Bou-Rabee, J. Sanz-Serna, Geometric integrators and the Hamiltonian Monte Carlo method, *Acta Numerica* 27 (2018) 113–206.

- [15] B. Jourdain, T. Lelièvre, B. Miasojedow, Optimal scaling for the transient phase of Metropolis Hastings algorithms: The longtime behavior, *Bernoulli* 20 (2014) 1930–1978.
- [16] B. Jourdain, T. Lelièvre, B. Miasojedow, Optimal scaling for the transient phase of the random walk Metropolis algorithm: The mean-field limit, *The Annals of Applied Probability* 25 (2015) 2263–2300.
- [17] C. C. Potter, R. H. Swendsen, 0.234: The Myth of a Universal Acceptance Ratio for Monte Carlo Simulations, *Physics Procedia* 68 (2015) 120–124.
- [18] A. Durmus, E. Moulines, M. Pereyra, Efficient bayesian computation by proximal markov chain monte carlo: when langevin meets moreau, *SIAM Journal on Imaging Sciences* 11 (1) (2018) 473–506.
- [19] P. Chaudhari, A. Oberman, S. Osher, S. Soatto, G. Carlier, Deep relaxation: partial differential equations for optimizing deep neural networks, *Research in the Mathematical Sciences* 5 (3) (2018) 30.
- [20] P. Chaudhari, A. Choromanska, S. Soatto, Y. LeCun, C. Baldassi, C. Borgs, J. Chayes, L. Sagun, R. Zecchina, Entropy-sgd: Biasing gradient descent into wide valleys (2016). [arXiv:arXiv:1611.01838](https://arxiv.org/abs/1611.01838).
- [21] A. Beskos, N. Pillai, G. Roberts, J.-M. Sanz-Serna, A. Stuart, Optimal tuning of the hybrid monte carlo algorithm, *Bernoulli* 19 (5A) (2013) 1501–1534.

## Appendix A. Details of mean square displacement computation

In this section, we give details of the derivation of (2.13). Differentiating (2.12) with respect to  $\sigma$

$$M' = \mathbb{E}_\mu \left[ \int |x - y|^2 (F'(R)\partial_\sigma Rg(y; x, \sigma) + F(R)\partial_\sigma g(y; x, \sigma)) dy \right] \quad (\text{A.1})$$

$$F'(r) = F(r)(1 - F(r)) \quad (\text{A.2})$$

$$\partial_\sigma R = \frac{\sigma}{4} (|\nabla V(x)|^2 - |\nabla V(y)|^2), \quad (\text{A.3})$$

$$\begin{aligned} \partial_\sigma g &= -\frac{n}{\sigma} g \\ &+ \frac{1}{\sigma^3} \left( |y - x + \frac{\sigma^2}{2} \nabla V(x)|^2 - 2(y - x + \frac{\sigma^2}{2} \nabla V(x)) \cdot \frac{\sigma^2}{2} \nabla V(x) \right) g. \end{aligned} \quad (\text{A.4})$$

Consequently,

$$\begin{aligned} M' &= \frac{\sigma}{4} \mathbb{E} [|x - y|^2 F(1 - F) (|\nabla V(x)|^2 - |\nabla V(y)|^2)] - \frac{n}{\sigma} M \\ &+ \frac{1}{\sigma^3} \mathbb{E} [|x - y|^2 F |y - x + \frac{\sigma^2}{2} \nabla V(x)|^2] \\ &- \frac{2}{\sigma^3} \mathbb{E} [|x - y|^2 F (y - x + \frac{\sigma^2}{2} \nabla V(x)) \cdot \frac{\sigma^2}{2} \nabla V(x)]. \end{aligned} \quad (\text{A.5})$$

Assuming that the optimal  $\sigma$  occurs at a finite value, the first order condition  $M' = 0$  will hold. (A.5), at the optimal value, can then be expressed as

$$M = \frac{1}{\sigma^2 n} \mathbb{E} \left[ |x - y|^2 F \left( |x - y|^2 - |\frac{\sigma^2}{2} \nabla V(x)|^2 F - |\frac{\sigma^2}{2} \nabla V(y)|^2 (1 - F) \right) \right]. \quad (\text{A.6})$$

This makes use of the identity

$$\begin{aligned} &|y - x + \frac{\sigma^2}{2} \nabla V(x)|^2 - 2(y - x + \frac{\sigma^2}{2} \nabla V(x)) \cdot \frac{\sigma^2}{2} \nabla V(x) \\ &= |y - x|^2 - |\frac{\sigma^2}{2} \nabla V(x)|^2. \end{aligned} \quad (\text{A.7})$$

Since  $M = \mathbb{E}[|x - y|^2 F]$ , we can re-express (A.6) to get (2.13).

## Appendix B. Details of computations in the dimension $n = 1$

In this section, we provide a derivation of (2.27). Let  $g_x(x)$  be the Gaussian density for  $N(0, k^{-1})$  and  $g_y(y|x)$  the Gaussian density for  $N((1 - \sigma^2 k/2)x, \sigma^2)$ . Then,

$$\begin{aligned} \text{MSD} &= \mathbb{E}[(y - x)^2 1 \wedge e^{R(x, y)}] = \int_{R(x, y) > 0} (y - x)^2 g_x(x) g_y(y|x) dx dy \\ &+ \int_{R(x, y) \leq 0} (y - x)^2 e^{R(x, y)} g_x(x) g_y(y|x) dx dy. \end{aligned} \quad (\text{B.1})$$

Next we observe that

$$(x - y)^2 e^{R(x,y)} g_x(x) g_y(y|x) = (x - y)^2 g_x(y) g_y(x|x). \quad (\text{B.2})$$

Furthermore we note that the set  $R(x,y) > 0$  corresponds to  $|x| > |y|$  and  $R(x,y) < 0$  corresponds to  $|x| < |y|$ . We can thus use the symmetry  $(x,y) \mapsto (y,x)$  to reduce (B.1) to

$$\begin{aligned} \text{MSD} &= 2 \int_{R(x,y)>0} (y - x)^2 g_x(x) g_y(y|x) dx dy \\ &= \int_{x=-\infty}^{\infty} \int_{y=-|x|}^{|x|} 2(y - x)^2 g_x(x) g_y(y|x) dx dy \\ &= \underbrace{\int_{x=-\infty}^0 \int_{y=x}^0 (\dots) dy dx}_{I} + \underbrace{\int_{x=-\infty}^0 \int_{y=0}^{-x} (\dots) dy dx}_{II} \\ &\quad + \underbrace{\int_{x=0}^{\infty} \int_{y=-x}^0 (\dots) dy dx}_{III} + \underbrace{\int_{x=0}^{\infty} \int_{y=0}^x (\dots) dy dx}_{IV}. \end{aligned} \quad (\text{B.3})$$

Since the integrand,  $2(y - x)^2 g_x(x) g_y(y|x)$  is invariant to  $(x,y) \mapsto (-x,-y)$ ,  $I = IV$  and  $II = III$ . Thus

$$\text{MSD} = 4 \int_{x=0}^{\infty} \int_{y=-x}^x g_x(x) g_y(y|x) dx dy. \quad (\text{B.4})$$

Using Mathematica and making the change of variables,  $\xi = \sqrt{k}x$  and  $\delta = k\sigma^2/2$ ,  $\text{MSD} = k^{-1}m(\delta)$  and

$$m(\delta) = \frac{2\delta}{\pi(4 + \delta(-2 + \delta))} \left\{ (8 + \delta^3) \arctan \left( \sqrt{\frac{8}{\delta^3}} \right) - 2\sqrt{2}\delta^{3/2} \right\} \quad (\text{B.5})$$

This function is plotted in Figure B.11.

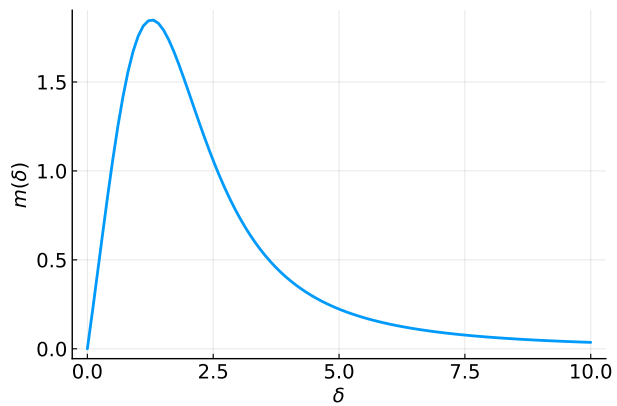


Figure B.11: Function (B.5). Note that it has a single maximum at  $\delta_* = 1.2779727440041808$ .